

## STED microscopy resolves nanoparticle assemblies

K I Willig, J Keller, M Bossi and S W Hell<sup>1</sup>

Department of NanoBiophotonics, Max Planck Institute for Biophysical Chemistry, D-37070 Göttingen, Germany  
E-mail: [hell@nanoscopy.de](mailto:hell@nanoscopy.de)

*New Journal of Physics* **8** (2006) 106

Received 9 May 2006

Published 22 June 2006

Online at <http://www.njp.org/>

doi:10.1088/1367-2630/8/6/106

**Abstract.** We demonstrate the ability of stimulated emission depletion (STED) microscopy, a far-field fluorescence imaging technique with diffraction-unlimited resolution, to reveal the spatial order of fluorescent nanoparticles. Unlike its confocal counterpart, here STED microscopy resolves the arrangements of densely packed 40 nm beads, supramolecular aggregates in a cell membrane, and colloidal nanoparticles. Both raw and linearly deconvolved data disclose unprecedented details of both biological and non-biological nanopatterns.

Abbe's discovery of the diffraction barrier has led to the popular notion that a far-field light microscope cannot resolve spatial structures that are smaller than about half of the wavelength of light [1]. In consequence, this insight triggered the invention of electron, x-ray, and scanning near-field optical microscopy (SNOM) [2, 3]. For many years after its invention, the latter seemed to be the only option to overcome the diffraction barrier in the optical domain [4]. To this end, SNOM employs either a tiny aperture or a nanometre-sized tip to confine the light-object interactions to subwavelength dimensions. Although it can accommodate most optical contrast modes, SNOM suffers from a number of drawbacks. While aperture-based SNOM entails feeble signals, its (plasmon and nonlinearly enhanced) tip counterpart requires a tight control of the tip-sample distance for artefact-free operation [5, 6]. In any case, SNOM is undeniably confined to the imaging of surfaces.

For many applications in biology and chemistry, it is certainly more desirable to break the diffraction barrier in the far-field. This formidable problem has been addressed several times in the 20th century, but effective methods have emerged only recently [7, 8]. Stimulated emission depletion (STED) microscopy overcomes the resolution-limiting role of diffraction for fluorescent samples. The idea underlying this concept can also be expanded to other contrast modes, provided they involve a reversible saturable optical transition [9, 10]. Nonetheless, being unrivalled in specificity and sensitivity, fluorescence is the most important non-invasive imaging

<sup>1</sup> Author to whom any correspondence should be addressed.

mode at the micron and submicron scale. Here, we demonstrate the power of STED microscopy to image the arrangement of densely packed fluorescent nanoparticles.

The key element of STED microscopy is a saturated depletion of the fluorescent state of the marker molecule [7, 11], whereby the depletion is accomplished with a focal intensity distribution featuring a local zero, e.g. a doughnut. The typical optical cross-sections and spontaneous relaxation times of a fluorophore dictate that STED is implemented optimally with picosecond excitation pulses that are swiftly followed by red-shifted 100–200 ps pulses for de-excitation [7, 11, 12]. Under these conditions, the population of a typical fluorescent marker decreases nearly exponentially with the energy of the stimulating pulse [13]. Oversaturating STED with sufficiently bright pulses confines the remaining fluorescence to the local zero. The net result is a subdiffraction-sized fluorescent focal spot [12]. Scanning this spot across the sample and registering the fluorescence renders subdiffraction images. This spot is tantamount to the effective point-spread-function (PSF) of the STED microscope,  $h_{\text{Eff}}(\vec{r})$ , giving the probability that a fluorescent molecule located at  $\vec{r}$  contributes to the measured signal. With  $h_{\text{Exc}}(\vec{r})$  and  $h_{\text{STED}}(\vec{r})$  describing the excitation PSF and STED-PSF, respectively, we obtain

$$h_{\text{Eff}}(\vec{r}) = h_{\text{Exc}}(\vec{r}) \exp[-\sigma h_{\text{STED}}(\vec{r}) \Phi_{\text{max}}]. \quad (1)$$

The PSFs are normalized to unity and  $\sigma$  is the cross-section for stimulated emission at the used wavelength. The flux  $\Phi_{\text{max}}$  gives the number of photons per area per pulse found at the local maximum bordering the zero, i.e. at the doughnut crest. The presence of a local ‘zero’,  $h_{\text{STED}}(0) = 0$ , implies that the fluorescence emission at  $\vec{r} \neq 0$  is increasingly suppressed with increasing  $\Phi_{\text{max}}$ , whereas that from  $\vec{r} = 0$  remains unaffected. Thus, the STED-PSF confines the effective PSF to a region that is much narrower than the excitation spot. In fact, equation (1) makes evident that  $h_{\text{Eff}}(\vec{r})$  can be narrowed down to a profile of arbitrarily small full-width-half-maximum (FWHM), although both the FWHM of  $h_{\text{Exc}}(\vec{r})$  and  $h_{\text{STED}}(\vec{r})$  are limited by diffraction. Calculations show that the FWHM of a STED-microscope [9, 10, 14],  $\Delta r$ , follows

$$\Delta r \cong \frac{\lambda}{2n \sin \alpha \sqrt{1 + \zeta}}, \quad (2)$$

with  $\zeta \equiv \Phi_{\text{max}} \sigma$  denoting the ‘saturation factor’ of the depletion. The expression  $n \sin \alpha$  gives the numerical aperture (NA) at which the focal doughnut is generated.

In our experiments, we employed a pulsed laser diode (Picoquant, Berlin, Germany) for excitation, emitting  $\sim 100$  ps pulses at  $\lambda_{\text{Exc}} = 470$  nm. The pulses were synchronized with yellow STED pulses ( $\lambda = 580\text{--}620$  nm) from a frequency-doubled optical parametric oscillator (OPO) system operating at 80 MHz. Featuring a spectral width of  $\sim 6$  nm, the  $\sim 250$  fs OPO pulses were downchirped in a single-mode optical fibre to  $\sim 200$  ps duration. The planar wavefront leaving the fibre was subjected to a helical phase delay  $P(\phi) = \exp(i\phi)$ , with  $0 < \phi < 2\pi$  being an angle centred around the optic axis. The phase delay was realized using a spatial phase modulator (Hamamatsu, Hamamatsu City, Japan) located optically conjugate to the entrance pupil of the lens. The objective lens (NA = 1.4 oil immersion, HCX PL APO, 100 $\times$ , by Leica, Mannheim, Germany) transformed this wavefront into a doughnut in the focal plane.

Figure 1 depicts the excitation spot (a), measured with a scattering 80 nm gold bead, together with the helical phase ramp (b) and the doughnut (c) for  $\lambda = 585$  nm; the latter serves as the STED-PSF  $h_{\text{STED}}(\vec{r})$ . Figure 1(e) shows the intensity profile  $h_{\text{STED}}(y = 0)$ , disclosing a central minimum of 160 nm FWHM and  $h_{\text{STED}}(0) = 0.015$ . Circular polarization of the pulses ensured

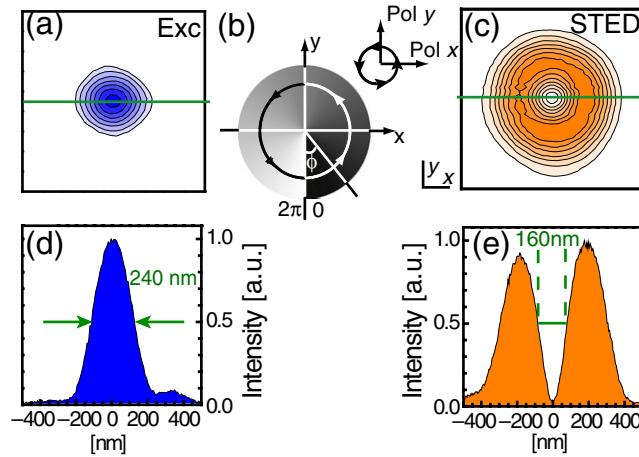


**Figure 1.** Creating the effective PSF of a single point scanning STED microscope: (a) excitation PSF at 470 nm, (b) helical phase ramp in the entrance pupil of a lens yields (c) the STED doughnut in the focal plane at 585 nm wavelength. Panels (d) and (e) display the profiles of (a) and (c), respectively, along the lines indicated. All PSFs are measured and drawn to scale.

that the marker molecules were stimulated irrespective of their transition dipole orientation in the focal plane. The observed residual asymmetry of the doughnut is due to wavefront aberrations of the lens as well as to imperfections of the spatial phase modulator. The shape of the excitation PSF is of lesser importance, since the periphery of the excitation spot is quenched.

Our choice of wavelengths aimed at dyes emitting in the green [15]. The circular opening of the photodetector covered 71% of the imaged Airy disk which is the most common setting in confocal microscopy. To account for this optional confocalization, the right-hand side of equation (1) is multiplied with the detection PSF given by the convolution of the lens PSF,  $h_{\text{Fl}}(\vec{r})$ , at the central emission wavelength  $\lambda_{\text{fl}}$ , with the image of the detector aperture in the focal plane

$$h_{\text{Eff}}(\vec{r}) = h_{\text{Exc}}(\vec{r}) \exp[-h_{\text{STED}}(\vec{r})\zeta][h_{\text{Fl}}(\vec{r}) \otimes \text{circ}(R)]. \quad (3)$$

$R$  denotes the radius of the imaged aperture. The primary reason for confocalization was to reject ambient light. The second reason was that blocking the STED beam,  $h_{\text{STED}}(\vec{r}) \equiv 0$ , instantly provided the confocal mode as a reference.

To demonstrate the potential of STED microscopy for nanoparticle imaging, we dispersed 40 nm yellow-green fluorescent beads (Molecular Probes, Eugene, OR) on a cover slip. The sample was mounted in Mowiol (Merck, Darmstadt, Germany), a polyvinylalcohol-based mounting medium. Tuned to  $\lambda = 585$  nm, the doughnut featured an average power of 42 mW yielding  $\Phi_{\text{max}} = 1.75 \times 10^{18}$  photons  $\text{cm}^{-2}$  per pulse in the focal plane. The comparison of the confocal image, figure 2(a), with its STED counterpart (b) demonstrates that, unlike confocal microscopy, STED microscopy identifies every 40 nm bead. The subdiffraction resolution is also evident in the line profiles (c), showing that beads separated by a 85 nm centre-to-centre distance are clearly resolved by an intensity dip of 45%. Both images were recorded simultaneously, by alternating the imaging mode every other line along the  $y$ -axis. This procedure ensured fair comparison of the two imaging modes. The pixel size was  $15 \times 15$  nm and the pixel dwell time was 0.2 ms.

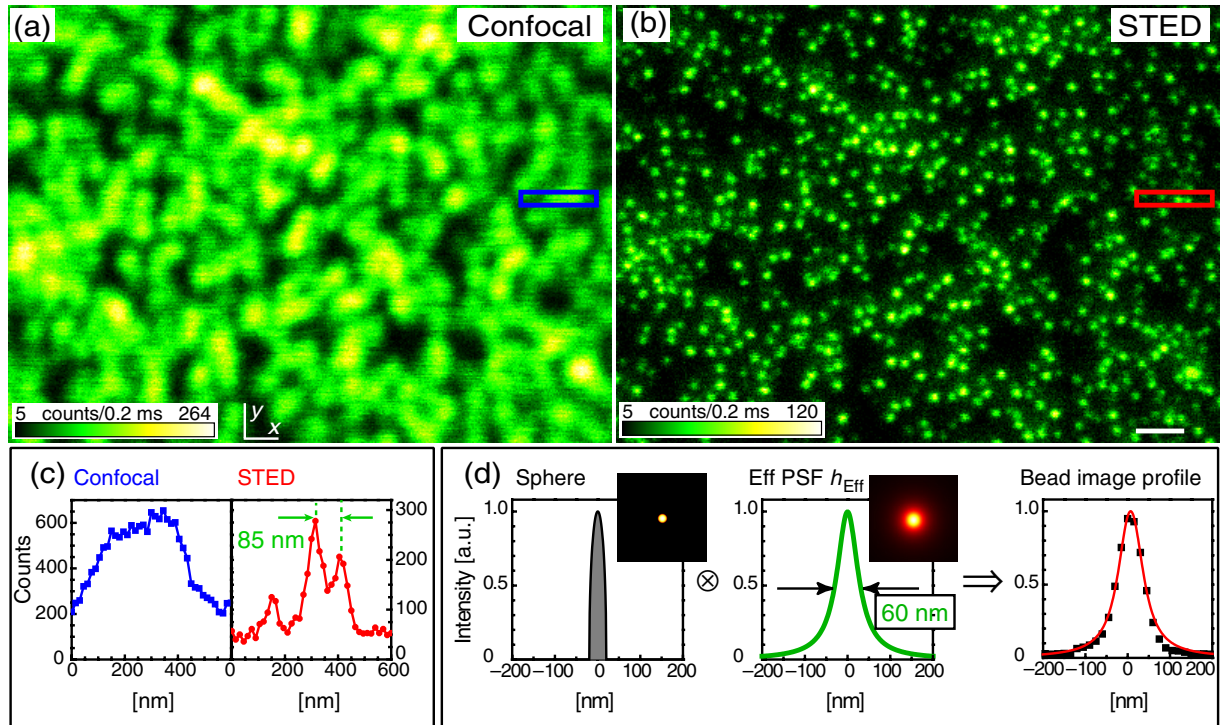


**Figure 2.** Subdiffraction resolution in the far-field. (a) Confocal versus (b) corresponding STED image of dispersed 40 nm beads. Scale bar = 500 nm (c) shows intensity profiles along the lines indicated in (a, b) (sum of 5 lines). Panel (d) establishes the effective resolution in the STED image, by taking advantage of the known bead size: the image of a bead (right) is given by the convolution of the object function (left) with the (initially unknown) effective PSF  $h_{\text{Eff}}$  of the STED microscope.  $h_{\text{Eff}}$  was established by fitting the result (red line) to the measured bead image profile (dotted). The resolution in (b) is all-physical. Note the ability of STED microscopy to resolve virtually every 40 nm bead individually. (See also [movie 1](#).)

The images of individual beads in figure 2(b) do not *a priori* represent the effective PSF  $h_{\text{Eff}}(\vec{r})$  of our STED recording, because the 40 nm bead size is not negligible. However, since the bead diameter is known, and since uniform fluorophore concentration in the bead can be assumed,  $h_{\text{Eff}}(\vec{r})$  can be extracted by deconvolving the image of a bead with the known object function (figure 2(d)). For that reason, we averaged individual bead images; the average profile is shown on the right-hand panel of figure 2(d). The centre panel shows the resulting  $h_{\text{Eff}}(\vec{r})$  featuring a FWHM of 60 nm. This value is >3-fold below the resolution limit of a confocal microscope and 4 times below the measured FWHM of the excitation light. Since the FWHM reduction is a reduction in diameter, the area of the spot decreased 9-fold as compared to confocal microscopy, thus explaining the dramatic visual improvement in the STED image.

Ideally, repeated excitation and de-excitation should not augment photobleaching. We have observed photobleaching amplification at elevated  $\Phi$ ; however it can be kept at moderate levels if the STED pulses are >150 ps [16]. The figure panels also indicate the signal strength in the respective images. For example, in the confocal and STED image of figure 2, we obtained a global maximum of 259 and 115 counts per pixel, respectively. The counts would have

been the same for both imaging modes if the 40 nm beads were point-like and the doughnut minimum  $h_{\text{STED}}(0)$  were perfectly zero. Nonfulfilment of the latter condition reduces the signal by  $1 - \exp[-\zeta h_{\text{STED}}(0)] = 0.14$ , using the independently measured value  $\zeta = 10$ . The majority of the higher maximum signal of confocal microscopy stems from the fact that more than just a single bead falls within the range of the confocal spot, thus adding signal from many beads. Imaging an isolated point-like object should have provided the same signal in both recordings. Nevertheless, depending on the fluorophore and the illumination scheme (pulse duration, etc) the total bleaching rate can be larger in the STED case [16].

Next we imaged self-assembling colloidal silica nanospheres on the surface of a glass cover slip. The nanospheres were prepared with a fluorescent core (figure 3(a)), following a protocol that produced highly monodispersed particles [17]. First, a small silica core of 50 nm diameter was prepared according to a water-in-oil microemulsion technique [18]. The particles were then grown to 68 nm including Atto532 (Attotec, Siegen, Germany), a Rhodamine related dye emitting a yellowish (540–620 nm) fluorescence. Finally, the beads were grown to a final diameter of 132 nm with a non-fluorescent shell, yielding a minimum separation of 64 nm between the fluorescent cores of the spheres [17]. All diameters were determined by electron microscopy. The STED beam was adjusted to 14 mW of average power and was tuned to  $\lambda = 615$  nm. Whereas the confocal image (figure 3(b)) is almost featureless, the STED image in figure 3(c) fully disclosed the semi-crystalline order of the nanoparticles. In particular, grain boundaries, point defects, disclinations and dislocations became clearly visible.

STED microscopy does not require any mathematical postprocessing. Still, one can take advantage of its optical transfer function (OTF) to strengthen the higher spatial frequencies gained by STED, employing a linear deconvolution. The OTF is obtained by a Fourier transformation of the effective PSF  $h_{\text{Eff}}(\vec{r})$ , which, unlike in the confocal microscope, depends on the saturation factor  $\zeta$  and hence on the dye in use. Therefore, we established  $h_{\text{Eff}}(\vec{r})$  for Atto532, and, for the same power, using single labelled antibodies (size  $<15$  nm). The result is shown in figure 3(d) along with the associated OTF. Both the FWHM of 67 nm, as well as the enlarged OTF, mark a substantial gain in optical bandwidth. The subsequent linear deconvolution of the STED image using a regularized Tikhonov–Miller algorithm [19] yields significantly improved image contrast (figure 3(e)).

We also deconvolved the confocal image, as shown in the inset of figure 3(b). However, the deconvolved confocal image still failed to resolve the nanoparticles, let alone the crystal defects. In fact, even the ‘raw’ STED image provides a higher resolution. Changing the physics of image formation is more powerful than deconvolution alone.

Finally, we imaged the nanoscale arrangement of the protein SNAP-25 on the plasma membrane of a fixed neuronal cell. A part of the SNARE protein family, SNAP-25 co-determines the membrane site at which a vesicle may dock and fuse. To visualize its spatial distribution, we labelled the protein with primary and Atto532-stained secondary antibodies. Again, the STED image (figure 4(b)) exhibits a detailed view of the protein spatial order. As in figure 3, the inset pictures display data obtained after linear deconvolution [19]. Figure 4(b) reveals for the first time that SNAP-25 is not randomly spread out on the plasma membrane, but organized in clusters of  $<60$  nm in size, which has important implications for synaptic transmission in neurons [20]. Thus STED not only provides subdiffraction images but also new biological insights, to be discussed elsewhere.

Equation (1) implies that STED microscopy neither relies on single-spot scanning nor on confocalization, because  $h_{\text{STED}}(\vec{r}) = 0$  may be prepared at multiple coordinates  $\vec{r}$ . The

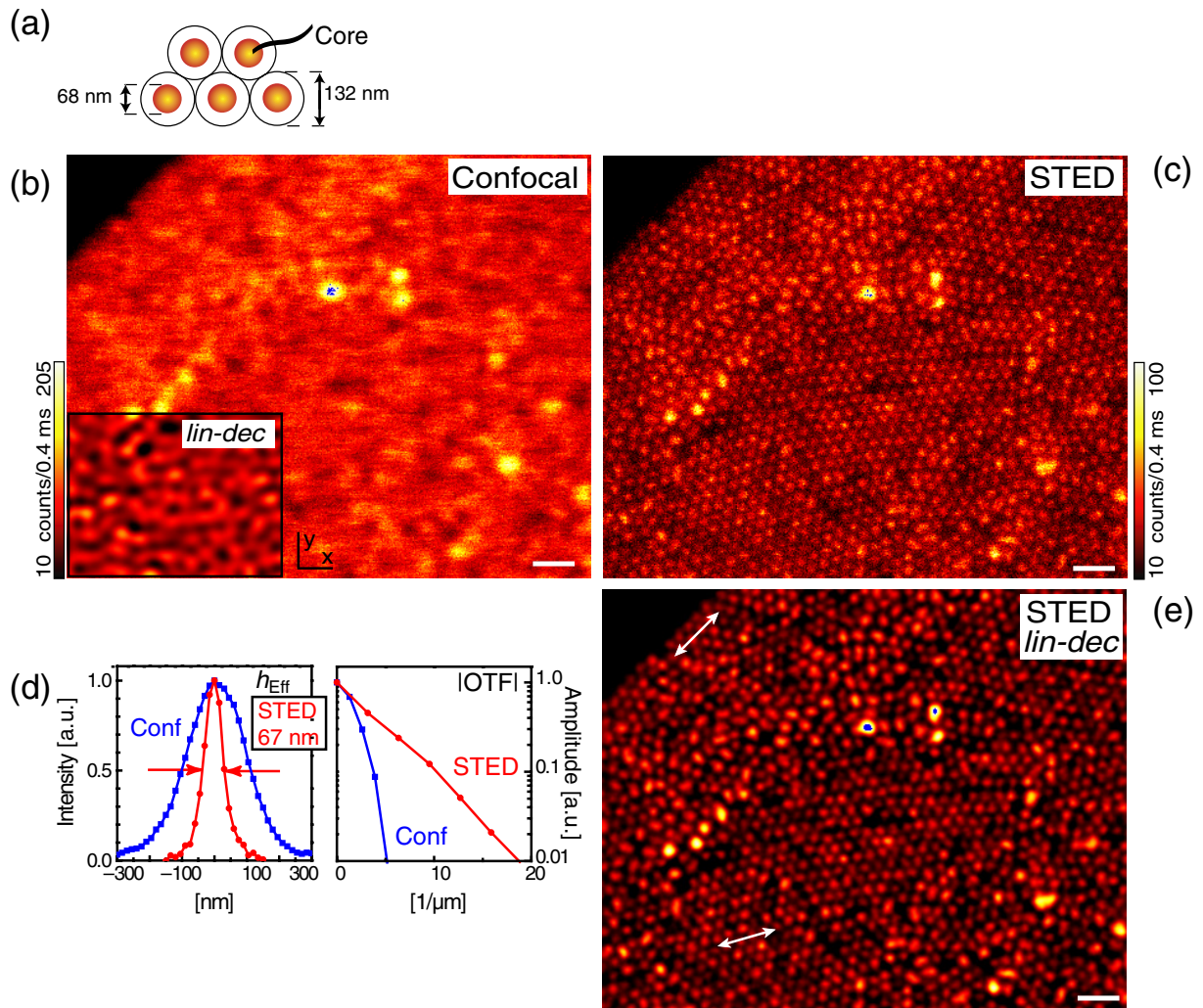


**Figure 3.** Imaging the spatial order of colloidal nanoparticles. (a) Sketch of silica nanoparticles featuring a fluorescent shell core; (b) confocal image, (c) corresponding STED image, (d) the effective PSF and OTF, determined from fluorescent point-objects of the same fluorophore as in the core, are utilized to enhance the STED image by linear deconvolution; the result is displayed in panel (e). For comparison, the inset of panel (b) shows the linearly deconvolved confocal data. Notwithstanding this, only the STED images (c) and (e) reveal grain boundaries, defects and dislocations in the semi-crystalline nanoparticle formation. Arrows to guide the eye; scale bars = 500 nm.

method can be parallelized using many zero points or lines to produce multiple subdiffraction-sized fluorescence spots or lines at the sample [10]. The fluorescence from these ultrasharp spots/lines can be registered in parallel by a camera, as in conventional microscopy, provided that they are further apart from each other than Abbe's barrier  $\Delta d = \lambda_n / (2n \sin \alpha)$ . Unlike in an epifluorescence microscope, the 'picture' on the camera is not the final image; it is just the fluorescence signal stemming from the subdiffraction dots/lines, blurred by diffraction. However, due to the gaps  $\Delta d$ , the blurred dot/line signal can be individually attributed to each

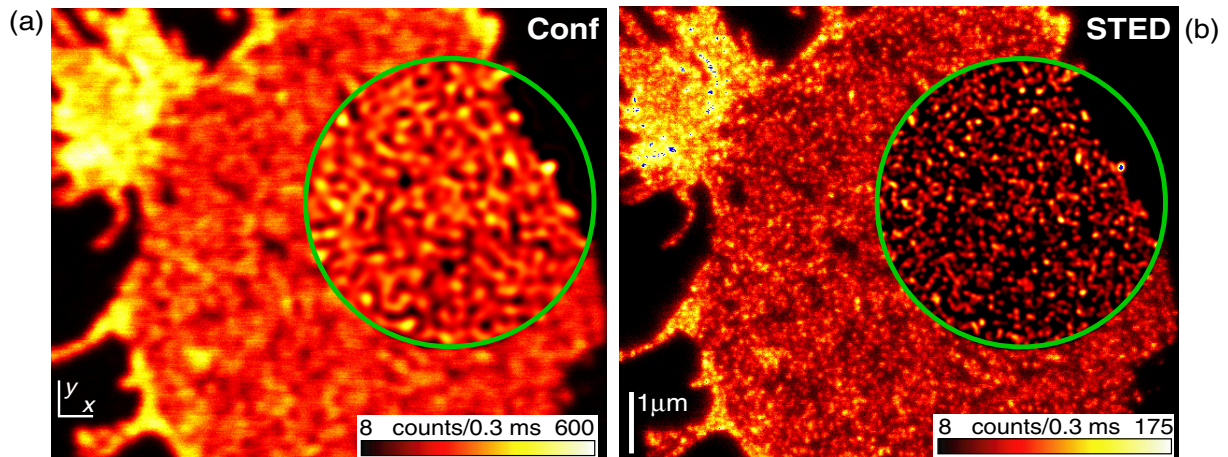


**Figure 4.** Revealing the nanopattern of the SNARE protein SNAP-25 on the plasma membrane of a mammalian cell. Confocal (a) versus STED image (b) of the antibody-tagged proteins. The encircled areas show linearly deconvolved data. STED microscopy provides a substantial leap forward in the imaging of protein self-assembly; here it reveals for the first time that SNAP-25 is ordered in clusters of  $<60$  nm average size. (See also [movie 2](#).)

subdiffraction sized spot/line at the sample. Storing this data and scanning the pattern further finally yields the subdiffraction image [10]. Therefore, while camera recording is possible within the framework of STED microscopy, scanning zero(s) through the specimens remains mandatory, even if the scanning is performed by shifting patterns of zeros in space [21].

The advantages of using a single spot instead of lines are that the resolution increase is uniform in all lateral directions, the desired image is attained as the spot scans, and no mathematical assignment is required. This is unlike in a remarkable recent study [21] in which subdiffraction resolution is obtained by depleting the ground state of the dye through hard absorption pumping and simultaneous observation of the saturated fluorescence signal [22]. With STED microscopy data, deconvolution is optional [23].

Powerful approaches exist to improve the axial resolution as well: the implementation of STED in a 4Pi-microscope [11, 13, 24] or the application of a further  $h_{\text{STED}}(\vec{r})$  with strong values above and beneath the focal plane [12]. The first alternative involves the addition of the aperture of two opposing lenses, whereas the latter can also be realized in a single lens. In fact, functions  $h_{\text{STED}}(\vec{r})$  have been described [12] which improved the axial resolution of a single lens by a factor of about six. As two STED pulses of different structure,  $h_{\text{STED}}(\vec{r})$ , can be applied simultaneously (within the lifetime of the fluorescent state), the spot can be squeezed both axially and laterally at the same time. Thus the nanoscale resolution of STED microscopy should be extendable to the imaging of three-dimensional (3D) colloidal crystals and other 3D-self assembling nanoparticles.

This avenue is particularly striking, since with the exception of perhaps x-ray imaging [25] (requiring a synchrotron), STED and related concepts currently are the only options available to non-destructively disclose the structure of photonic crystals and of other nanoparticle assemblies in 3D. Due to the recently demonstrated macromolecular-scale resolution potential [14], STED microscopy is likely to undergo improvements that should fundamentally enhance the imaging studies shown herein.

## Acknowledgments

We thank Professor A van Blaaderen for showing us the preparation of fluorescent silica nanoparticles. MB acknowledges a Marie Curie postdoctoral fellowship by the European Union. We acknowledge the SNAP-25 preparation by J Sieber and T Lang and A Schönle for his software Inspector. We also thank B Rankin for critical reading. SWH acknowledges a grant by the German Ministry of Education and Research.

## References

- [1] Abbe E 1873 *Arch. f. Mikroskop. Anat.* **9** 413–20
- [2] Pohl D W, Denk W and Lanz M 1984 *Appl. Phys. Lett.* **44** 651–3
- [3] Lewis A, Isaacson M, Harootunian A and Murray A 1984 *Ultramicroscopy* **13** 227–31
- [4] Betzig E and Chichester R J 1993 *Science* **262** 1422–5
- [5] Novotny L, Hecht B and Pohl D W 1998 *Ultramicroscopy* **71** 341–4
- [6] Frey H G, Keilmann F, Kriele A and Guckenberger R 2002 *Appl. Phys. Lett.* **81** 5030–2
- [7] Hell S W and Wichmann J 1994 *Opt. Lett.* **19** 780–2
- [8] Hell S W and Kroug M 1995 *Appl. Phys. B* **60** 495–7
- [9] Hell S W 2004 *Phys. Lett. A* **326** 140–5
- [10] Hell S W 2003 *Nature Biotechnol.* **21** 1347–55
- [11] Hell S W 1997 Increasing the resolution of far-field fluorescence light microscopy by point-spread-function engineering *Topics in Fluorescence Spectroscopy* vol 5, ed J R Lakowicz (New York: Plenum) pp 361–422
- [12] Klar T A, Jakobs S, Dyba M, Egner A and Hell S W 2000 *Proc. Natl Acad. Sci. USA* **97** 8206–10
- [13] Dyba M and Hell S W 2002 *Phys. Rev. Lett.* **88** 163901
- [14] Westphal V and Hell S W 2005 *Phys. Rev. Lett.* **94** 143903
- [15] Willig K I, Rizzoli S O, Westphal V, Jahn R and Hell S W 2006 *Nature* **440** 935–9
- [16] Dyba M and Hell S W 2003 *Appl. Opt.* **42** 5123–9
- [17] van Blaaderen A and Vrij A 1992 *Langmuir* **8** 2921–31
- [18] Osseo-Asare K and Arriagada F J 1990 *Colloids Surf.* **50** 321–39
- [19] Tikhonov A N and Arsenin V Y 1977 *Solutions of Ill-Posed Problems* (New York: Wiley)
- [20] Sieber J J, Willig K I, Heintzmann R, Hell S W and Lang T 2006 *Biophys. J.* **90** 2843–51
- [21] Gustafsson M G L 2005 *Proc. Natl Acad. Sci. USA* **102** 13081–6
- [22] Heintzmann R, Jovin T M and Cremer C 2002 *J. Opt. Soc. Am. A: Opt. Image Sci. Vision* **19** 1599–609
- [23] Westphal V, Seeger J, Salditt T and Hell S W 2005 *J. Phys. B: At. Mol. Opt. Phys.* **38** S695–S705
- [24] Dyba M, Jakobs S and Hell S W 2003 *Nature Biotechnol.* **21** 1303–4
- [25] Kipp L, Skibowski M, Johnson R L, Berndt R, Adelung R, Harm S and Seemann R 2001 *Nature* **414** 184–8